EurJIC European Journal of Inorganic Chemistry
ChemPubSoc Europe
FULL PAPER

DOI:10.1002/ejic.201402495

Elucidating the Origin of Enhanced Phosphorescence Emission in the Solid State (EPESS) in Cyclometallated Iridium Complexes

Ashlee J. Howarth,[a] Raissa Patia,[b] David L. Davies,*[b] Francesco Lelj,*[c] Michael O. Wolf,*[a] and Kuldip Singh[b]

Keywords: EPESS / Phosphorescence / Density functional calculations / Pi interactions / Iridium

A new mechanism for enhanced phosphorescence emission in the solid state (EPESS) in cyclometallated Ir complexes with the general formula $[Ir(C^{\wedge}N)_2(N^{\wedge}O)]$ involving distortion of the six-membered chelate ring of the ancillary ligand is proposed. Photophysical and computational studies show that neither π-stacking nor restricted rotation cause the observed EPESS in these complexes and that ligand distortions in the triplet excited state are responsible for EPESS

Introduction

Organic light-emitting diodes (OLEDs) and light-emitting electrochemical cells (LECs) require molecules that emit intensely in the solid state.[1,2] Interactions between molecules in the solid state are known to influence emission behaviour. Typically, molecules that are strongly emissive in dilute solution become less emissive in concentrated solutions or in the solid state due to "aggregation caused quenching" (ACQ).[3] In 2001, Tang and co-workers reported a series of substituted 2,3,4,5-tetraphenylsiloles in which aggregation caused an enhancement in emission in the solid state compared to dilute solution, a phenomenon they dubbed "aggregation induced emission" (AIE).[4,5] Since this discovery, many organic chromophores exhibiting AIE have been reported.[6] Recently, coordination complexes of iridium,[7] platinum[8] and rhenium[9] that show AIE have also been reported. In such complexes, emission often arises from states with triplet character, so AIE in this class of compounds is also called enhanced phosphorescence emission in the solid state (EPESS). The performance of solid-state molecular devices depends strongly on the molecular assembly of components. As a consequence, understanding and controlling molecular arrangements in the solid state is pertinent to these applications.[10]

EPESS in metal complexes has been attributed to a variety of factors including restricted intramolecular rotation (RIR),[11] or π-stacking.[7] However, the complexity of the excited state manifolds in these complexes makes unambiguous determination of the origin of EPESS difficult. Cyclometallated iridium complexes are of particular interest due to their high photoluminescence efficiencies and the ability to colour tune their emission.[12] Two different mechanisms have been proposed to drive EPESS in cyclometallated iridium complexes. One mechanism involves restricted intramolecular rotations of substituents on the bidentate ancillary ligand ($N^{\wedge}O$[11] or $N^{\wedge}N$[13]) and the other involves π-stacking of cyclometallating phenylpyridine ligands.[7,14,15]

Park et al. proposed that restricted intramolecular rotation around the N–aryl bond of salicylimine ligands in the solid state suppresses a non-radiative decay pathway giving rise to EPESS.[11] The solid-state absorption and luminescence properties of **1**–**4** were studied in neat films as well as in various polymer films.[11] Due to the presence of strong solid-state emission in the polymer films of **1**–**4**, it was concluded that the solid-state emission does not arise from an excimeric or aggregated state.[11] Instead, a combination of low temperature emission and TD-DFT studies were used to conclude that rotation around the N–aryl bond in solution gives rise to a non-radiative decay pathway causing these complexes to be non-emissive in solution.[11] It was proposed that this pathway is slowed down or shut off in the solid state giving rise to the observed emission.[11]

Li et al. have suggested that π-stacking of phenylpyridine ligands lowers the energy of an emissive ^{3}MLLCT state below that of a non-emissive triplet ligand (^{3}L) state, resulting in an increase in emission in the solid state compared to solution.[7] This explanation was first proposed from studies of **5**–**7**, where **5** does not show EPESS in contrast to **6** and **7**.[7] The triplet energies of the ancillary ligands (^{3}L) of **5**–**7**

[a] Department of Chemistry, University of British Columbia
Vancouver, BC V6T 1Z1, Canada
E-mail: mwolf@chem.ubc.ca
http://groups.chem.ubc.ca/wolf/
[b] Department of Chemistry, University of Leicester
Leicester, LE1 7RH, UK
http://www2.le.ac.uk/departments/chemistry/people/academic-staff/david_l_davies
[c] Dipartimento di Scienze, Università della Basilicata
85100 Potenza, Italy
Supporting information for this article is available on the WWW under http://dx.doi.org/10.1002/ejic.201402495.

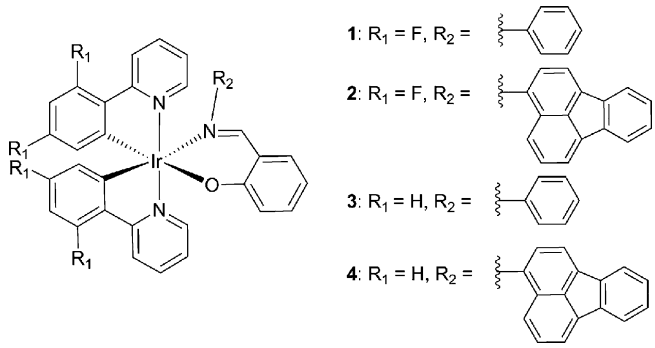

were measured and **6** and **7** were determined to have low-lying triplet energies.[7] From these results, it was proposed that π-stacking lowers an emissive ^{3}MLLCT state below the low-lying, non-emissive ^{3}L state (in **6** and **7**) giving rise to emission in the solid state.[7] Follow-up studies on **8**–**10** were used to dispute the theory of restricted rotation proposed by Park et al. since **8** and **9** have ancillary ligand substituents, which are not free to rotate yet still show EPESS.[15] Li et al. used X-ray crystallography[7,15] as well as emission spectroscopy on micro-aggregates formed in acetonitrile/water mixtures,[7] to suggest that the phenylpyridine ligands π-stack and give rise to the solid-state emission observed.

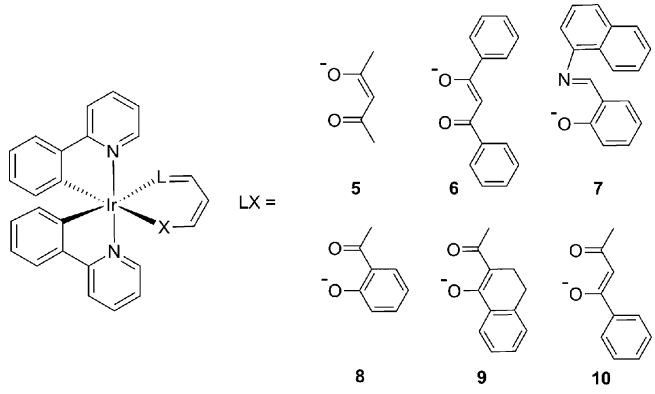

There are some contradictory results in the data reported by Park and Li respectively which suggest that neither of the interpretations proposed by these groups is correct. Park et al. have shown that strong solid-state emission is observed in polymer films[11] (when π-stacking interactions are diminished[16]). This observation is inconsistent with the interpretation put forward by Li et al. as the cause of EPESS. The studies by Li et al. in which strong solid-state emission is observed in complexes with ancillary ligand substituents unable to rotate[15] do not support Park's hypothesis of how EPESS is generated. Herein, we propose a new mechanism to explain EPESS in cyclometallated Ir complexes with the general formula [Ir(C^N)$_2$(N^O)] (**3**, **4**, **7** and **11**–**17**). Using a combination of photophysical and computational studies we show that neither π-stacking nor restricted rotation of ancillary ligand substituents cause the observed EPESS in these complexes. Rather, we propose that the cause of EPESS in these complexes is a distortion of the bonding of the six-membered chelate ring of the ancillary ligand to the metal atom. We show that this also applies to [Ir(C^N)$_2$(O^O)] complexes and hence is consistent with all the experimental observations made previously by Park[11] and Li[7,15] and may apply more widely to other transition metal complexes.

Results and Discussion

Synthesis and Photophysical Properties

Complexes **3**, **4**, **7** and **11**–**17** were studied to test the effect of restricted N–aryl and N–alkyl rotations as well as π-stacking on EPESS. Increasing steric bulk of the R group from phenyl to fluoranthyl to 2,6-diisopropylphenyl was used to test the effects of restricted N–R rotation. Ir^{III} complexes with phenylpyrazole cyclometallating ligands were used as a starting point to test the effects of π-stacking on EPESS, since phenylpyrazole ligands have been shown to be less likely than phenylpyridine ligands to π-stack in the solid state.[17] Complexes **3**, **4**, **7** and **11**–**17** were prepared by treating the appropriate Ir^{III} dimer with the corresponding salicylimine proligand under microwave irradiation at 100 °C for 30 min. All complexes were characterized by high resolution mass spectrometry and ^{1}H NMR spectroscopy (COSY, NOESY, TOCSY and HSQC) allowing full assignment of all resonances. X-ray crystal structures were also obtained for **15**–**17**.

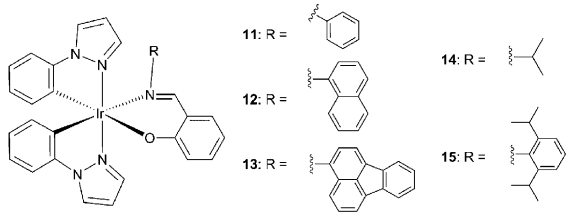

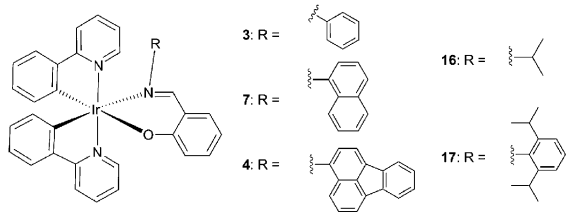

Complexes **3**, **4**, **7** and **11**–**17** show either very weak or no phosphorescence at room temperature in dichloromethane solution (Figure S1, Supporting Information). In stark contrast to this observation, all of the complexes display enhanced phosphorescence emission in the solid state in both powder and crystalline forms. A thin film of each complex was prepared by drop casting of dichloromethane solutions of **3**, **4**, **7** and **11**–**17** onto a glass slide and emission was observed with λ_{max} between 580 and 635 nm, measured at 298 K (Figure 1). Although the solid-state quantum yields

are not particularly high, these complexes still display EPESS and can be used to study the mechanism that drives this phenomenon.

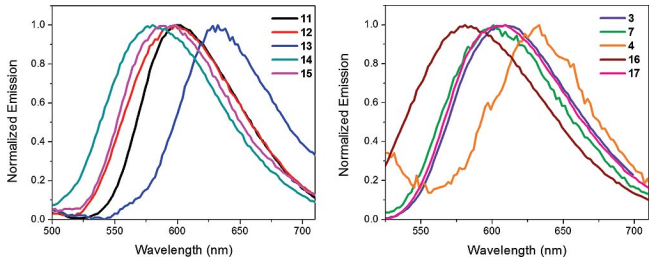

Figure 1. Solid-state emission spectra of **3**, **4**, **7** and **11**–**17**, λ_{ex} = 400 nm.

Effects of Restricted Rotation

Previously, restricted intramolecular rotation around the N–aryl bond of the salicylimine ligand in the solid state was proposed to suppress a non-radiative decay pathway giving rise to EPESS.[11] Contrary to this proposal, our results show that there is no correlation between the size of the substituent on the salicylimine ligand and the presence or absence of emission in solution. In addition, there is no correlation between size and the emission quantum yield of the complex in the solid state (Table 1). If rotation around the N–aryl (or N–alkyl) bond was giving rise to a non-radiative pathway, then complexes in which rotation is hindered or fixed would be expected to be emissive in solution and hence not show significant EPESS. The ^{1}H NMR spectrum of **15** shows four inequivalent doublets (δ = 1.18, 1.03, 0.87 and 0.62 ppm) corresponding to the methyl groups of the isopropyl substituents as well as two septets (δ = 3.48 and 2.68 ppm) corresponding to the CH groups of the isopropyl substituents; complex **17** shows similar features. The observation of inequivalent diisopropyl substituents on the diisopropylphenyl moiety confirms that there is no rotation of the N–aryl substituent on the NMR timescale, yet complexes **15** and **17** still demonstrate EPESS. These results, as well as others reported in the literature showing complexes with fixed substituents that display EPESS,[15] confirm that restricted rotation around the N–aryl bond is not the major cause of EPESS in these complexes.

Table 1. Solid-state emission wavelengths and quantum yields of neat solids and solids in a PMMA matrix. Measurements taken in air.

Complex	Solution λ_{em}	Solution f	Solid λ_{em}	Solid f	PMMA λ_{em}	PMMA f
3	–	–	609	0.058	570	0.134
4	–	–	633	0.012	604	0.097
7	–	–	600	0.045	576	0.096
11	–	–	602	0.080	578	0.086
12	–	–	598	0.044	574	0.139
13	–	–	632	0.014	604	0.086
14	589	0.013	580	0.028	559	0.047
15	593	<< 0.001[a]	592	0.049	569	0.099
16	584	<< 0.001[a]	581	0.036	534	0.117
17	–	–	607	0.028	570	0.109

[a] Quantum yield was too low to be accurately measured.

Effects of π-Stacking

To test the possible effects of π-stacking[7,15] or aggregation in complexes **3**, **4**, **7** and **11**–**17**, 2 wt.-% of each complex was dispersed into a PMMA matrix, allowing isolation of the molecules from one another in the solid state.[16] In all ten complexes, the solid-state emission maxima in PMMA are blueshifted by 21–47 nm (Figure 2) compared to the corresponding complexes in the undiluted solid state (Table 1). Redshifts in solid-state absorption and emission spectra are typically observed due to intermolecular interactions,[18] and the blueshifts observed here confirm that intermolecular solid-state interactions are less prevalent when the complexes are placed in the polymer matrix (i.e. the molecules are more isolated). In addition, in each case, the emission quantum yield of the complex in PMMA is higher than that of the solid (Table 1), demonstrating that the solid-state emission is partially quenched in the aggregated form. These results are consistent with the more common aggregation caused quenching (ACQ) effect[3] and demonstrate that π-stacking or aggregation of these complexes in the solid state is not giving rise to EPESS. In fact, π-stacking or aggregation is actually detrimental to the enhancement of the emission observed. In addition, the π-stacking that has been previously reported[7,15] always involved phenylpyridine cyclometallating ligands. We also observe EPESS behaviour in complexes bearing phenylpyrazole ligands which typically do not show long-range π-stacking in the solid state.[17]

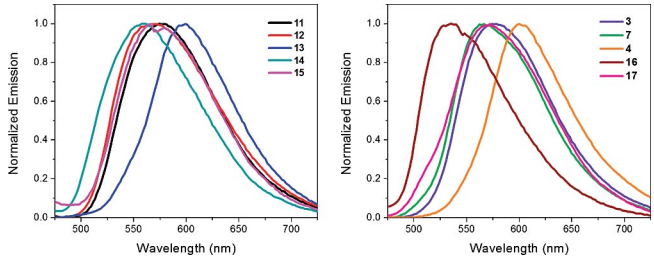

Figure 2. Solid-state emission spectra of **3**, **4**, **7** and **11**–**17** in a PMMA matrix.

X-ray Crystallography

The X-ray structures of **15**–**17** have been determined, and they all show the expected atom connectivities. The structure of **15** is shown in Figure 3 and those for **17** and **16** are in Figures S2 and S3, respectively (Supporting Information). Diagrams showing a lack of evidence for π-stacking in all three structures are provided in Figure S4 (Supporting Information). The Ir–N(salicylimine) bond, where the N atom is *trans* to the C atom of the cyclometallating ligand, is much longer than the Ir–N(ppy/ppz) bonds. In complex **15** the phenylpyrazole of one molecule is coplanar

with that of another (Figure S4a, Supporting Information) although the two planes are considerably offset with only minor overlapping of the two pyrazole rings (centroid–centroid distance of 3.42 Å). The plane of the N^O ligand (N,C,C,C,O) is considerably distorted from the IrC_2 plane forming an interplanar angle of 27.6° (Figure 3). The corresponding phenylpyridine complex **17** shows some π-stacking of the phenylpyridine ligands, which are at an angle of 7.1° to each other although again the rings are offset from one another (centroid–centroid distance of pyridine in one molecule and phenyl in another is 4.16 Å). The angle between the plane of the N^O ligand and IrC_2 plane is 24.5° (Figure S2, Supporting Information). In complex **16**, the phenylpyridine ligands in adjacent molecules are almost coplanar but are hardly overlapped (centroid–centroid distance of pyridine in one molecule and pyridine in another is 3.80 Å). The angle between the plane of the N^O ligand and IrC_2 plane is 22.2° (Figure S3, Supporting Information). Overall, there is very little evidence in any of these structures for a significant degree of π-stacking. A notable feature in all three cases is the bending of the N^O plane away from the IrC_2 plane. The reasons for this are not obvious. However, there are a number of weak interactions between molecules in the solid state. For example, in **15** there are close contacts between the salicylimine phenol ring and the C–H bond of a pyrazole, and of an isopropyl group, from two different adjacent molecules. In all cases, these short contacts suggest restricted motion of the molecules in the solid state.

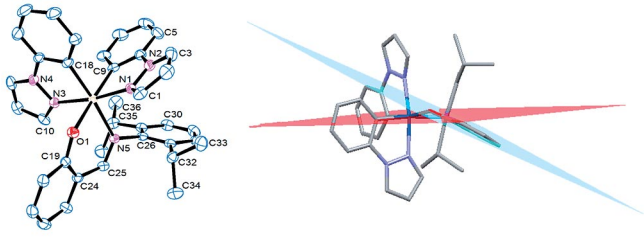

Figure 3. ORTEP and wireframe representation of **15** showing the angle between the IrC_2 and N^O plane.

DFT Calculations

To better understand the emission observed in complexes such as **3**, **4**, **7** and **11**–**17** detailed DFT calculations were carried out. TD-DFT calculations show that the lowest energy triplet consists mainly of a LUMO–HOMO transition justifying the use of an unrestricted DFT (UDFT) approach to study the first triplet state. UDFT calculations of **3**, **4**, **7** and **11**–**17** reveal that the HSOMO and HSOMO-1[19] contain both Ir metal character as well as contributions from each of the three ligands (Figure 4 and S5 in Supporting Information), consistent with emission from a ^{3}MLLCT state. This suggests that the nature of both the cyclometallating ligands as well as the ancillary N^O ligand is important for the observed emission. DFT results show that the emission from **13** and **4** is redshifted relative to the other complexes whereas **14** and **16** are blueshifted. This is due to a shift in the LUMO from being localized on the salicylimine portion of the N^O ancillary ligand (blueshift) to being delocalized onto the N–aryl moiety of the N^O ancillary ligand (redshift).

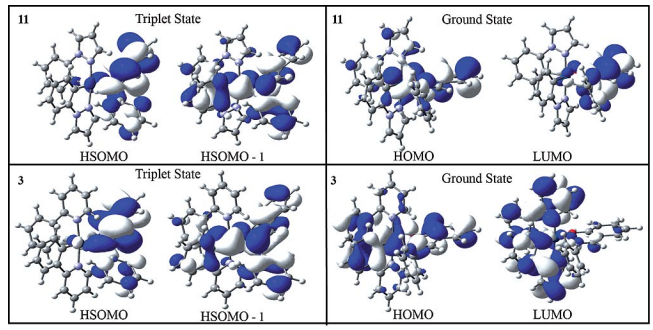

Figure 4. HSOMO-1 (α) and HSOMO (α) images as well as ground-state frontier molecular orbital images from unrestricted DFT (UDFT) and TD-DFT calculations respectively for **11** and **3**. HSOMO: Highest Singly Occupied Molecular Orbital.

DFT and UDFT calculations were performed to help understand the origins of EPESS. For complex **11**, the ground-state calculation shows that in the most stable structure the plane of the phenol imine ligand and the equatorial[20] plane are almost coplanar (angle between planes = 5.94°). However, in the triplet excited state the phenol imine tilts with respect to the equatorial plane leading to two stable conformations of this state [tilted up (43.54°) or down (–25.65)]. The cause of this distortion can be traced to the fact that the LUMO has antibonding character between Ir and the phenol imine ligand. Thus, the plane of the phenol imine tilts with respect to the equatorial plane to reduce antibonding interactions and to allow population of this orbital in the triplet excited state (T_1). Hence, the conformers do not arise from a distortion of the phenol imine ancillary ligand. Rather, the distortion is in how this ligand bonds to the metal atom. This ligand distortion does not require a rotatable imine substituent, therefore EPESS in complexes that do not have rotatable groups can also be explained by this mechanism. The largest barrier separating the two conformers of **11** is only 15.7 kJ/mol (Figure 5), and, as a result, they can rapidly interconvert in solution at room temperature. This geometric change in the excited state gives rise to a non-radiative decay pathway which deactivates the ^{3}MLLCT state in solution at room temperature. Similar distortions were observed in complexes **3**, **4**, **7** and **12**–**17** (Figure S7, Supporting Information), suggesting that the non-radiative decay pathway has the same origin in all cases. Ligand distortions in solution have been reported as the cause of non-radiative decay in a series of EPESS-active Pt complexes containing similar N^O chelating ligands.[21,22] Calculations that simulate a solid-state matrix (see Supporting Information), show that the T_1 state is much less distorted than in solution. This leads to an

enhancement in the contribution of the Franck–Condon factor for the ^{3}MLLCT emission and hence makes this transition more likely in the solid state.

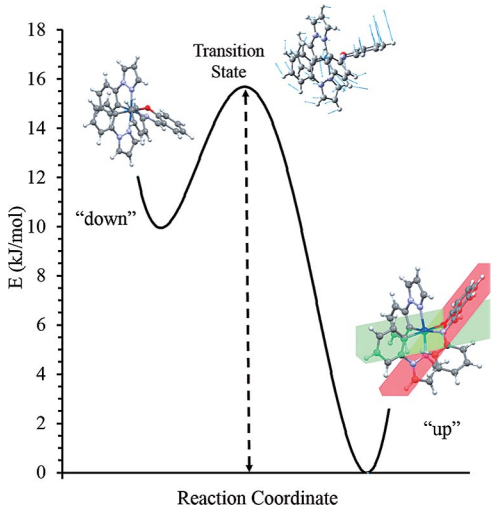

Figure 5. Computed energy profile for the excited triplet state geometry of **11** relative to the half chair inversion of the six-membered ring. The green plane is the equatorial plane, and the red plane is the phenol imine ligand plane. Blue arrows show the transition vectors related to the interconversion between minima and are associated with the imaginary frequency of 23.72i cm^{-1}.

In addition to Ir^{III} complexes with N^O ligands, complexes with O^O ancillary ligands have also been shown to demonstrate EPESS and to be of interest in OLED applications.[7,12,17c,23] To further test our theory, calculations were performed on a series of known complexes (**5**, **6**, **18**, and **19**) containing bidentate O^O ancillary ligands. These complexes also contain ancillary ligands with six-membered chelate rings and **6**, **18** and **19** have been shown to demonstrate EPESS.[7,12,17c,23]

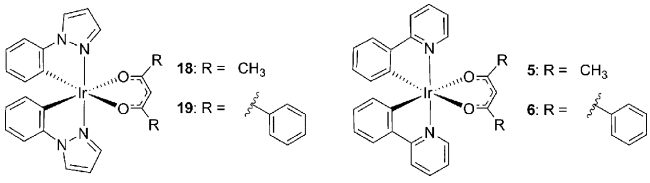

Complex **18** demonstrates EPESS,[17c,23] whereas complex **5** is strongly emissive in both solution and the solid state[7,12] and therefore fails to display EPESS. Calculations of **18** show that ligand distortions occur in the excited triplet state, which is in agreement with our interpretation (Figure 6). Calculations of **5**, however, show that ligand distortions do not occur in the excited triplet state, and instead the acac ancillary ligand remains planar with respect to the equatorial plane (Figure 6). This is convincing evidence that excited state ligand distortions give rise to EPESS. Complexes **6** and **19** both demonstrate EPESS[7,12,23] and consistent with our interpretation, calculations show that both complexes undergo excited state ligand distortions (Figure S8, Supporting Information).

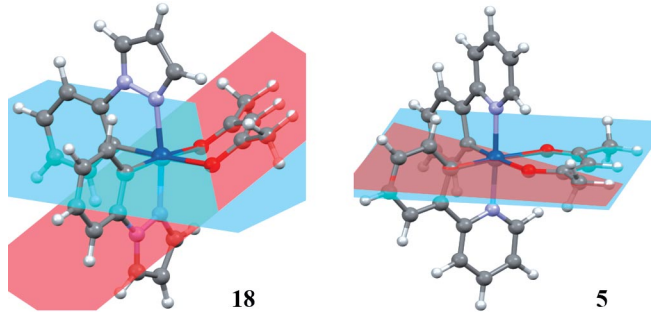

Figure 6. Excited triplet state geometry of **18** and **5**. The green plane is the equatorial plane, and the red plane is the acac ligand plane.

In the complexes demonstrating EPESS (**3**, **4**, **6**, **7** and **11**–**19**), the ground-state HOMO and/or LUMO must contain significant contributions from the N^O or O^O ancillary ligand (Figures 4, S5 and S9). In complex **5**, which does not show EPESS, the HOMO and LUMO do not show any contribution from the acac ancillary ligand. Although the origins of the excited state ligand distortions are very complex, these results suggest that involvement of the ancillary ligand is a prerequisite for distortion to occur.

Conclusions

Most examples of EPESS-active iridium complexes in the literature contain ancillary ligands bound through a flexible six-membered chelate ring.[7,14,15] This suggests that distortions of the ancillary ligand relative to the equatorial plane may more broadly serve as the origin of EPESS in such complexes. The use of six-membered rings may therefore be a useful design criterion for the synthesis of EPESS-active complexes. The few EPESS-active complexes that contain a five-membered chelate,[13,24] have very bulky ancillary ligand substituents, and, in these cases, EPESS is almost certainly due to restricted rotation. The relative energies of the cyclometallating and ancillary ligands are likely also important since the emission results from a ^{3}MLLCT state involving orbitals on all three ligands. Additionally, it is important to ensure that the transition involves orbitals that have a significant contribution from the atoms of the six-membered chelate ring and not orbitals exclusively on the C^N ligands and/or the periphery of the complex.

Experimental Section

General: All experiments were performed under nitrogen, using standard Schlenk-line techniques. Deuterated solvents were purchased from Cambridge Isotope Laboratories Inc. Chloro(1-phenylpyrazole)iridium(III) dimer $[IrCl(ppz)_2]_2$,[25] chloro(2-phenylpyridine)iridium(III) dimer $[IrCl(ppy)_2]_2$,[25] 2-[(phenylimino)methyl]-phenol (NOPh),[11] 2-[(1-naphthalenylimino)methyl]phenol (NONapht),[26] 2-[(3-fluoranthenylimino)methyl]phenol (NOFluor),[11] and 2-({[2,6-bis(1-methylethyl)phenyl]imino}methyl)phenol (NO*i*Prop$_2$Ph)[27] were prepared according to literature procedures. 2-{[(1-Methylethyl)imino]methyl}phenol (NO*i*Prop) was prepared by

a typical Schiff base condensation reaction in ethanol. All other solvents and reagents were obtained from commercial sources and used as received. ^{1}H NMR and ^{13}C NMR spectra were obtained using a Bruker AV-400 spectrometer and referenced to the residual protonated solvent peak. NMR spectra were assigned using a combination of COSY, NOESY, TOCSY and HSQC experiments. Electrospray ionization mass spectrometry data were obtained with a Bruker Esquire LC ion trap mass spectrometer. Microwave reactions were performed with a Biotage Initiator 2.5 microwave synthesizer. Fluorescence spectroscopy data were collected using a Photon Technology International QuantaMaster fluorimeter. Solid-state emission spectra were obtained at 298 K by drop-casting a dichloromethane solution of each complex onto a glass slide. Absolute quantum yields were determined with an integrating sphere coupled to the PTI fluorimeter. Neat solid quantum yields were obtained from drop-casting of a dichloromethane/hexane (1:1) solution of each complex. PMMA matrix quantum yields were drop-cast from dichloromethane.

X-ray Diffraction: Data were collected with a Bruker Apex 2000 CCD diffractometer using graphite monochromated Mo-K_α radiation (λ = 0.7107 Å). The data were corrected for Lorentz and polarisation effects, and empirical absorption corrections were applied. The structure was solved by direct methods and with structure refinement on F^2 employing SHELXTL version 6.10.[28] Hydrogen atoms were included in calculated positions (C–H 0.95–1.00 Å, O–H 0.84 Å) riding on the bonded atom with isotropic displacement parameters set to 1.5U_{eq}(O) for hydroxy H atoms, 1.5U_{eq}(C) for methyl hydrogen atoms and 1.2U_{eq}(C) for all other H atoms. All non-hydrogen atoms were refined with anisotropic displacement parameters without positional restraints. Disordered solvent in **16** was removed using the Squeeze option in PLATON.[29] Figures were drawn using the program ORTEP.[30] CCDC-987738 (**15**), CCDC-987739 (**16**), CCDC-987737 (**17**), contain the supplementary crystallographic data for this paper. These data can be obtained free of charge from The Cambridge Crystallographic Data Centre via www.ccdc.cam.ac.uk/data_request/cif.

Synthesis of Ir(ppy)$_2$(NOPh) (3): This complex has been reported previously[11] using different synthetic procedures. [IrCl(ppy)$_2$]$_2$ (0.070 g, 0.065 mmol), NOPh (0.028, 0.14 mmol) and sodium carbonate (0.015 g, 0.14 mmol) were placed in a microwave vial with ethanol (3.5 mL). The suspension was degassed with nitrogen for 4 min. The vial was placed in the microwave reactor and heated under microwave irradiation at 100 °C (18 bar, 155 W) for 30 min. The solvent was then removed in vacuo and the solid residue dissolved in CH_2Cl_2 (10 mL). The resulting yellow solution was passed through a Celite pad and the filtrate reduced to approximately 2 mL in volume. Layering with hexanes yielded the desired product as an orange-yellow precipitate. The product was purified by column chromatography using CH_2Cl_2 to elute any unreacted NOPh and then EtOAc/CH_2Cl_2 (1:1) to elute complex **3** (0.026 g, yield 29%).

Synthesis of Ir(ppy)$_2$(NOFluor) (4): This complex has been reported previously[11] using different synthetic procedures. [IrCl(ppy)$_2$]$_2$ (0.070 g, 0.065 mmol), NOFluor (0.046, 0.14 mmol) and sodium carbonate (0.015 g, 0.14 mmol) were placed in a microwave vial with ethanol (3.5 mL). The suspension was degassed with nitrogen for 4 min. The vial was placed in the microwave reactor and heated under microwave irradiation at 100 °C (18 bar, 155 W) for 30 min. The solvent was then removed in vacuo and the solid residue dissolved in CH_2Cl_2 (10 mL). The resulting yellow-brown solution was passed through a Celite pad and the filtrate reduced to approximately 2 mL in volume. Layering with hexanes yielded the desired product as a dark orange precipitate. The product was purified by column chromatography using CH_2Cl_2 to elute any unreacted NOFluor and then EtOAc/CH_2Cl_2 (1:1) to elute complex **4** (0.040 g, yield 38%).

Synthesis of Ir(ppy)$_2$(NONapht) (7): This complex has been reported previously[7] using different synthetic procedures. [IrCl(ppy)$_2$]$_2$ (0.070 g, 0.065 mmol), NONapht (0.035, 0.14 mmol) and sodium carbonate (0.015 g, 0.14 mmol) were placed in a microwave vial with ethanol (3.5 mL). The suspension was degassed with nitrogen for 4 min. The vial was placed in the microwave reactor and heated under microwave irradiation at 100 °C (18 bar, 155 W) for 30 min. The solvent was then removed in vacuo and the solid residue dissolved in CH_2Cl_2 (10 mL). The resulting yellow-orange solution was passed through a Celite pad and the filtrate reduced to approximately 2 mL in volume. Layering with hexanes yielded the desired product as a yellow precipitate. The product was purified by column chromatography using CH_2Cl_2 to elute any unreacted NONapht and then EtOAc/CH_2Cl_2 (1:1) to elute complex **7** (0.036 g, yield 37%).

Synthesis of Ir(ppz)$_2$(NOPh) (11): [IrCl(ppz)$_2$]$_2$ (0.070 g, 0.068 mmol), NOPh (0.030, 0.15 mmol) and sodium carbonate (0.016 g, 0.15 mmol) were placed in a microwave vial with ethanol (3.5 mL). The suspension was degassed with nitrogen for 4 min. The vial was placed in the microwave reactor and heated under microwave irradiation at 100 °C (18 bar, 155 W) for 30 min. The solvent was then removed in vacuo and the solid residue dissolved in CH_2Cl_2 (10 mL). The resulting yellow solution was passed through a Celite pad and the filtrate reduced to approximately 2 mL in volume. Layering with hexanes yielded the desired product as a bright orange precipitate. The product was purified by column chromatography using CH_2Cl_2 to elute any unreacted NOPh and then EtOAc/CH_2Cl_2 (1:1) to elute complex **11** (0.031 g, yield 34%).

Synthesis of Ir(ppz)$_2$(NONapht) (12): [IrCl(ppz)$_2$]$_2$ (0.070 g, 0.068 mmol), NONapht (0.037, 0.15 mmol) and sodium carbonate (0.016 g, 0.15 mmol) were placed in a microwave vial with ethanol (3.5 mL). The suspension was degassed with nitrogen for 4 min. The vial was placed in the microwave reactor and heated under microwave irradiation at 100 °C (18 bar, 155 W) for 30 min. The solvent was then removed in vacuo and the solid residue dissolved in CH_2Cl_2 (10 mL). The resulting yellow-orange solution was passed through a Celite pad and the filtrate reduced to approximately 2 mL in volume. Layering with hexanes yielded the desired product as a bright yellow precipitate. The product was purified by column chromatography using CH_2Cl_2 to elute any unreacted NONapht and then EtOAc/CH_2Cl_2 (1:1) to elute complex **12** (0.029 g, yield 29%).

Synthesis of Ir(ppz)$_2$(NOFluor) (13): [IrCl(ppz)$_2$]$_2$ (0.070 g, 0.068 mmol), NOFluor (0.048, 0.15 mmol) and sodium carbonate (0.016 g, 0.15 mmol) were placed in a microwave vial with ethanol (3.5 mL). The suspension was degassed with nitrogen for 4 min. The vial was placed in the microwave reactor and heated under microwave irradiation at 100 °C (18 bar, 155 W) for 30 min. The solvent was then removed in vacuo and the solid residue dissolved in of CH_2Cl_2 (10 mL). The resulting yellow-brown solution was passed through a Celite pad and the filtrate reduced to approximately 2 mL in volume. Layering with hexanes yielded the desired product as a dark orange precipitate. The product was purified by column chromatography using CH_2Cl_2 to elute any unreacted NOFluor and then EtOAc/CH_2Cl_2 (1:1) to elute complex **13** (0.046 g, yield 43%).

Synthesis of Ir(ppz)$_2$(NO*i*Prop) (14): [IrCl(ppz)$_2$]$_2$ (0.070 g, 0.068 mmol), NO*i*Prop (0.024, 0.15 mmol) and sodium carbonate

(0.016 g, 0.15 mmol) were placed in a microwave vial with ethanol (3.5 mL). The suspension was degassed with nitrogen for 4 min. The vial was placed in the microwave reactor and heated under microwave irradiation at 100 °C (18 bar, 155 W) for 30 min. The solvent was then removed in vacuo and the solid residue dissolved in CH_2Cl_2 (10 mL). The resulting yellow-brown solution was passed through a Celite pad and the filtrate reduced to approximately 2 mL in volume. Layering with hexanes yielded the desired product as a yellow precipitate. The product was purified by column chromatography using CH_2Cl_2 to elute any unreacted NO*i*-Prop and then EtOAc/CH_2Cl_2 (1:1) to elute complex **14** (0.040 g, yield 46%).

Synthesis of Ir(ppz)$_2$(NO*i*Prop$_2$Ph) (15): $[IrCl(ppz)_2]_2$ (0.070 g, 0.068 mmol), NO*i*Prop$_2$Ph (0.042, 0.15 mmol) and sodium carbonate (0.016 g, 0.15 mmol) were placed in a microwave vial with ethanol (3.5 mL). The suspension was degassed with nitrogen for 4 min. The vial was placed in the microwave reactor and heated under microwave irradiation at 100 °C (18 bar, 155 W) for 30 min. The solvent was then removed in vacuo and the solid residue dissolved in CH_2Cl_2 (10 mL). The resulting orange-brown solution was passed through a Celite pad and the filtrate reduced to approximately 2 mL in volume. Layering with hexanes yielded the desired product as an orange-yellow precipitate. The product was purified by column chromatography using CH_2Cl_2 to elute any unreacted NO*i*Prop$_2$Ph and then EtOAc/CH_2Cl_2 (1:1) to elute complex **15** (0.027 g, yield 26%).

Synthesis of Ir(ppy)$_2$(NO*i*Prop) (16): $[IrCl(ppy)_2]_2$ (0.070 g, 0.065 mmol), NO*i*Prop (0.023, 0.14 mmol) and sodium carbonate (0.015 g, 0.14 mmol) were placed in a microwave vial with ethanol (3.5 mL). The suspension was degassed with nitrogen for 4 min. The vial was placed in the microwave reactor and heated under microwave irradiation at 100 °C (18 bar, 155 W) for 30 min. The solvent was then removed in vacuo and the solid residue dissolved in CH_2Cl_2 (10 mL). The resulting yellow-brown solution was passed through a Celite pad and the filtrate reduced to approximately 2 mL in volume. Layering with hexanes yielded the desired product as a yellow precipitate. The product was purified by column chromatography using CH_2Cl_2 to elute any unreacted NO*i*Prop and then EtOAc/CH_2Cl_2 (1:1) to elute complex **16** (0.037 g, yield 43%).

Synthesis of Ir(ppy)$_2$(NO*i*Prop$_2$Ph) (17): $[IrCl(ppy)_2]_2$ (0.070 g, 0.065 mmol), NO*i*Prop$_2$Ph (0.040 g, 0.14 mmol) and sodium carbonate (0.015 g, 0.14 mmol) were placed in a microwave vial with ethanol (3.5 mL). The suspension was degassed with nitrogen for 4 min. The vial was placed in the microwave reactor and heated under microwave irradiation at 100 °C (18 bar, 155 W) for 30 min. The solvent was then removed in vacuo and the solid residue dissolved in CH_2Cl_2 (10 mL). The resulting yellow-orange solution was passed through a Celite pad and the filtrate reduced to approximately 2 mL in volume. Layering with hexanes yielded the desired product as an orange precipitate. The product was purified by column chromatography using CH_2Cl_2 to elute any unreacted NO*i*Prop$_2$Ph and then EtOAc/CH_2Cl_2 (1:1) to elute complex **17** (0.037 g, yield 37%).

DFT Calculations: Complexes **3**–**7**, and **11**–**19** were studied by ab initio DFT and TD-DFT methods. Preliminary calculations were performed using the widely diffused hybrid xc functional B3LYP;[31] this has been shown to have some drawbacks because of the wrong asymptotic behavior; therefore the 1 parameter xc functionals mPW1PW91[32] and the PB1PBE[33] and the more recent M06[34] meta-hybrid functional were also used. For all second-period atoms, the Dunning[35] all-electron basis set augmented by a set of d polarization functions [D95(d)] was used. Hydrogen atoms not involved in any hydrogen bonds were described by the same Dunning basis set that does not include p polarization functions. For Ir, the new double-ζ Stuttgart[36] basis set including f-polarization functions and relativistic effects by a fully relativistic small core pseudopotential[33] (SDD09) were used and not the default SDD as included in Gaussian 09, Revision C.01. The ultrafine option with 99590 grid points was used thoroughly for the integral calculations for all atoms except Ir, where a total of 1566228 grid points were used. The first triplet-state structure was computed using the unrestricted approach. All energy-minimized structures were characterized by the calculation of the Hessian matrix in order to check that they were minima and not simple stationary points on the molecular Born–Oppenheimer energy surface. Wavefunctions were checked against possible internal instability.[37,38] TD-DFT calculations were performed by increasing the initial configuration space for the Davidson[39] diagonalization, unlike the default option in the program. A dichloromethane solvent environment was simulated by the self-consistent reaction field.[40] The vibrational band structure was evaluated by computing the Frank–Condon contribution[41,42] between the ground-state S_0 structure and T_1 structures and their harmonic vibrational properties. Further T_1 structures were computed by constraining the O^N-Ph ligand conformation of the N–Ir–O–C and C–N–Ir–O dihedral as in the ground state, while optimizing all the remaining geometrical parameters to simulate the effect of the solid state constraining those internal degrees of freedom. All calculations were performed using Gaussian 09, Revision C.01.[43]

Supporting Information (see footnote on the first page of this article): NMR assignments, additional photophysical and crystallographic data and DFT calculations.

Acknowledgments

We thank the Natural Sciences and Engineering Research Council (NSERC) of Canada for funding this research. D. L. D. thanks the Leverhulme Trust for a Study Abroad Fellowship. F. L. thanks the National Interuniversity Consortium of Materials Science and Technology (INSTM) for financial support for a visiting leave from Italy.

[1] E. Holder, B. M. W. Langeveld, U. S. Schubert, *Adv. Mater.* **2005**, *17*, 1109–1121.
[2] M. A. Baldo, S. Lamansky, P. E. Burrows, M. E. Thompson, S. R. Forrest, *Appl. Phys. Lett.* **1999**, *75*, 4–6.
[3] J. B. Birks, in *Photophysics of Aromatic Molecules*, Wiley, London, **1970**.
[4] B. Z. Tang, X. Zhan, G. Yu, P. P. S. Lee, Y. Liu, D. Zhu, *J. Mater. Chem.* **2001**, *11*, 2974–2978.
[5] J. Luo, Z. Xie, J. W. Y. Lam, L. Cheng, H. Chen, C. Qiu, H. S. Kwok, X. Zhan, Y. Liu, D. Zhu, B. Z. Tang, *Chem. Commun.* **2001**, 1740–1741.
[6] a) Y. T. Wu, M. Y. Kuo, Y. T. Chang, C. C. Shin, T. C. Wu, C. C. Tai, T. H. Cheng, W. S. Liu, *Angew. Chem. Int. Ed.* **2008**, *47*, 9891–9894; *Angew. Chem.* **2008**, *120*, 10039; b) C. J. Bhongale, C. W. Chang, C. S. Lee, E. W. G. Diau, C. S. Hsu, *J. Phys. Chem. B* **2005**, *109*, 13472–13482.
[7] Q. Zhao, L. Li, F. Li, M. Yu, Z. Liu, T. Yi, C. Huang, *Chem. Commun.* **2008**, 685–687.
[8] M. X. Zhu, W. Lu, N. Y. Zhu, C. M. Che, *Chem. Eur. J.* **2008**, *14*, 9736–9746.
[9] B. Manimaran, P. Thanasekaran, T. Rajendran, R.-J. Lin, I.-J. Chang, G.-H. Lee, S.-M. Peng, S. Rajagopal, K.-L. Lu, *Inorg. Chem.* **2002**, *41*, 5323–5325.

[10] W. Jones, in *Organic Molecular Solids*, CRC Press, Boca Raton, **1997**.
[11] Y. You, H. S. Huh, K. S. Kim, S. W. Lee, D. Kim, S. Y. Park, *Chem. Commun.* **2008**, 3998–4000.
[12] S. Lamansky, P. Djurovich, D. Murphy, F. Abdel-Razzaq, H.-E. Lee, C. Adachi, P. E. Burrows, S. R. Forrest, M. E. Thompson, *J. Am. Chem. Soc.* **2001**, *123*, 4304–4312.
[13] G.-G. Shan, D.-X. Zhu, H.-B. Li, P. Li, Z.-M. Su, Y. Liao, *Dalton Trans.* **2011**, *40*, 2947–2953.
[14] H. Wu, T. Yang, Q. Zhao, J. Zhou, C. Li, F. Li, *Dalton Trans.* **2011**, *40*, 1969–1976.
[15] K. Huang, H. Wu, M. Sei, F. Li, T. Yi, C. Huang, *Chem. Commun.* **2009**, 1243–1245.
[16] T. Fukaminato, T. Umemoto, Y. Iwata, S. Yokojima, M. Yoneyama, S. Nakamura, M. Irie, *J. Am. Chem. Soc.* **2007**, *129*, 5932–5938.
[17] a) T.-H. Kwon, H. S. Cho, M. K. Kim, J.-W. Kim, J.-J. Kim, K. H. Lee, S. J. Park, I.-S. Shin, H. Kim, D. M. Shin, Y. K. Chung, J.-I. Hong, *Organometallics* **2005**, *24*, 1578–1585; b) A. B. Tamayo, S. Garon, T. Sajoto, P. I. Djurovich, I. M. Tsyba, R. Bau, M. E. Thompson, *Inorg. Chem.* **2005**, *44*, 8723–8732; c) L.-L. Wu, I.-W. Sun, C.-H. Yang, *Polyhedron* **2007**, *26*, 2679–2685; d) W. Jiang, Y. Gao, Y. Sun, F. Ding, Y. Xu, Z. Bian, F. Li, J. Bian, C. Huang, *Inorg. Chem.* **2010**, *49*, 3252–3260; e) K. Hanson, A. Tamayo, V. V. Diev, M. T. Whited, P. I. Djurovich, M. E. Thompson, *Inorg. Chem.* **2010**, *49*, 6077–6084; f) S. Kammer, I. Starke, A. Pietrucha, A. Kelling, W. Mickler, U. Schilde, C. Dosche, E. Kleinpeter, H.-J. Holdt, *Dalton Trans.* **2012**, *41*, 10219–10227; g) G.-G. Shan, H.-B. Li, H.-T. Cao, D.-X. Zhu, Z.-M. Su, Y. Liao, *J. Organomet. Chem.* **2012**, *713*, 20–26.
[18] S.-Y. Chang, J. Kavitha, S.-W. Li, C.-S. Hsu, Y. Chi, Y.-S. Yeh, P.-T. Chou, G.-H. Lee, A. J. Carty, Y.-T. Tao, C.-H. Chien, *Inorg. Chem.* **2006**, *45*, 137–146.
[19] HSOMO: Highest Singly Occupied Molecular Orbital.
[20] The equatorial plane refers to the plane defined by the cyclometallated phenyl C, the Ir and the N and O atoms of the salicylimine ligand (see Figure S6, Supporting Information).
[21] S. Liu, H. Sun, Y. Ma, S. Ye, X. Liu, X. Zhou, X. Mou, L. Wang, Q. Zhao, W. Huang, *J. Mater. Chem.* **2012**, *22*, 22167–22173.
[22] M. Ghedini, A. Golemme, I. Aiello, N. Godbert, R. Termine, A. Crispini, M. La Deda, F. Lelj, M. Amati, S. Belviso, *J. Mater. Chem.* **2011**, *21*, 13434–13444.
[23] a) L.-L. Wu, S.-H. Tsai, T.-F. Guo, C.-H. Yang, I.-W. Sun, *J. Lumin.* **2007**, *126*, 687–694; b) T. Fei, X. Gu, M. Zhang, C. Wang, M. Hanif, H. Zhang, Y. Ma, *Synth. Met.* **2009**, *159*, 113–118.
[24] a) G.-G. Shan, L.-Y. Zhang, H.-B. Li, S. Wang, D.-X. Zhu, P. Li, C.-G. Wang, Z.-M. Su, Y. Liao, *Dalton Trans.* **2012**, *41*, 523–530; b) G.-G. Shan, H.-B. Li, H.-Z. Sun, D.-X. Zhu, H.-T. Cao, Z.-M. Su, *J. Mater. Chem. C* **2013**, *1*, 1440–1449.
[25] D. L. Davies, M. P. Lowe, K. S. Ryder, K. Singh, S. Singh, *Dalton Trans.* **2011**, *40*, 1028–1030.
[26] W. Rodrıguez-Cordoba, J. S. Zugazagoitia, E. Collado-Fregoso, J. Peon, *J. Phys. Chem. A* **2007**, *111*, 6241–6247.
[27] L. Clowes, M. Walton, C. Redshaw, Y. Chao, A. Walton, P. Elo, V. Sumerin, D. L. Hughes, *Catal. Sci. Technol.* **2013**, *3*, 152–160.
[28] Bruker, version 6.10 ed., Bruker Inc, Madison, Wisconsin, USA, **1998–2000**.
[29] P. Vandersluis, A. L. Spek, *Acta Crystallogr., Sect. A* **1990**, *46*, 194.
[30] L. J. Farrugia, *J. Appl. Crystallogr.* **1997**, *30*, 565.
[31] A. D. Becke, *J. Chem. Phys.* **1997**, *107*, 8554–60.
[32] C. Adamo, V. Barone, *J. Comput. Chem.* **1998**, *19*, 418–29.
[33] C. Adamo, V. Barone, *J. Chem. Phys.* **1999**, *110*, 6158–69.
[34] Y. Zhao, D. G. Truhlar, *Theor. Chem. Acc.* **2008**, *120*, 215–241.
[35] T. H. Dunning Jr., P. J. Hay, in *Modern Theoretical Chemistry*, Plenum, New York, **1976**.
[36] D. Figgen, K. A. Peterson, M. Dolg, H. Stoll, *J. Chem. Phys.* **2009**, *130*, 164108.
[37] R. Bauernschmitt, R. Ahlrichs, *J. Chem. Phys.* **1996**, *104*, 9047–52.
[38] J. S. Sears, T. Koerzdoerfer, C. Zhang, J. L. Bredas, *J. Chem. Phys.* **2011**, *135*, 151103.
[39] E. R. Davidson, *J. Comp. Physiol.* **1975**, *17*, 87–94.
[40] J. Tomasi, B. Mennucci, R. Cammi, *Chem. Rev.* **2005**, *105*, 2999–3093.
[41] J. Weber, G. Hohlneicher, *Mol. Phys.* **2003**, *101*, 2125–44.
[42] F. Santoro, A. Lami, R. Improta, V. Barone, *J. Chem. Phys.* **2007**, *126*, 184102.
[43] M. J. Frisch, G. W. Trucks, H. B. Schlegel, G. E. Scuseria, M. A. Robb, J. R. Cheeseman, G. Scalmani, V. Barone, B. Mennucci, G. A. Petersson, H. Nakatsuji, M. Caricato, X. Li, H. P. Hratchian, A. F. Izmaylov, J. Bloino, G. Zheng, J. L. Sonnenberg, M. Hada, M. Ehara, K. Toyota, R. Fukuda, J. Hasegawa, M. Ishida, T. Nakajima, Y. Honda, O. Kitao, H. Nakai, T. Vreven, J. A. Montgomery Jr., J. E. Peralta, F. Ogliaro, M. Bearpark, J. J. Heyd, E. Brothers, K. N. Kudin, V. N. Staroverov, R. Kobayashi, J. Normand, K. Raghavachari, A. Rendell, J. C. Burant, S. S. Iyengar, J. Tomasi, M. Cossi, N. Rega, N. J. Millam, M. Klene, J. E. Knox, J. B. Cross, V. Bakken, C. Adamo, J. Jaramillo, R. Gomperts, R. E. Stratmann, O. Yazyev, A. J. Austin, R. Cammi, C. Pomelli, J. W. Ochterski, R. L. Martin, K. Morokuma, V. G. Zakrzewski, G. A. Voth, P. Salvador, J. J. Dannenberg, S. Dapprich, A. D. Daniels, Ö. Farkas, J. B. Foresman, J. V. Ortiz, J. Cioslowski, D. J. Fox, *Gaussian 09*, Revision C.01, Gaussian, Inc., Wallingford, CT, **2009**.

Received: June 2, 2014
Published Online: July 15, 2014

